CHAPTER-2

Experiments

This chapter begins with the selection of materials for designing desired interfaces among the three different types of engineering materials such as metals, ceramics and glasses. In order to attain the intended interfaces, various synthesis techniques have been chosen. Each and every synthesis method is described briefly in the subsequent sections. Synthesized interfaces have been investigated extensively using grazing incidence X-ray diffraction (GIXRD) and transmission electron microscope (TEM). Different modes of TEM characterization have been utilized and working details along with principles are given subsequently. Last section of this chapter ends with the discussion of the computational methods relevant to experimental results.

2.1 Materials systems

The material systems that have been selected in the present study can be categorized into three parts: 1) Metals, 2) ceramics and, 3) glasses. Such material systems may further be classified on the basis of nature of classification of interfaces. The interface classification has been done in this study on the basis of periodicity. Three types of interfaces studied here pertains to (i) crystalline/crystalline interfaces in metals, (ii) crystalline/crystalline interfaces in ceramics, and (iii) amorphous/crystalline interfaces in glasses.

Metallic materials chosen for designing the crystalline/crystalline interfaces in metal system are Au and Cu. Pure (> 99.5%) Au was procured in the form of gold coin (1 g) from P.C. Jewelers, Varanasi, India. Whereas Cu (>99.90) was given in the form of wire (0.5 mm diameter) by the Department of Electronics Engineering, IIT BHU, Varanasi, India.

In order to design the crystalline/crystalline interfaces in ceramics, Li based oxides such as $LiNiO_2$ and $LiMnO_x$ were procured. For the substrate material, single-crystal Nb-doped $SrTiO_3$ (Nb:STO) was selected. The $LiNiO_2$ and $LiMnO_x$ pallets and Nb:STO substrates were bought from Toshima Co. and Furuchima Chemical, respectively. The $SrTiO_3$ is known to be a good conductor and its conductivity enhances with Nb doping. It has been

used as a substrate with a view to exploit its superior conductivity. Amorphous/crystalline interfaces in a glassy material is the third interface to be investigated in this study. The material precursors used in synthesizing amorphous/crystalline interface are Fe-based amorphous powders and mild steel. Mild steel is used as a substrate material. Mild steel is chosen as they are quite prone to corrosion and degradation. It is being done to investigate improvement of a protective coating of amorphous-steel nanocomposites on corrosion and wear resistance properties.

2.2 Materials synthesis

As mentioned in the previous section, the three interfaces were synthesized through different routes. Multilayer thin film of Au and Cu was prepared by thermal evaporation technique to observe crystalline/crystalline interface. In contrast, the crystalline/crystalline interface involving ceramic materials was synthesized by pulsed laser deposition (PLD) technique. Ceramic materials such as $LiNiO_2$, $LiMnO_x$ were used as targets and Nb:STO was utilized as substrate. Combinatorial deposition technique was used to synthesize either compositionally graded or core-shell thin films.

Synthesis of amorphous/crystalline interface in the form of hard coating was done using the Fe-based amorphous powder and mild steel. Compositions for them are given in chapter 6 of this thesis. Fe-based amorphous/nanocomposite powder in the form of hard coating was deposited onto the mild steel substrate through high velocity oxy-fuel (HVOF) thermal spraying process. Prior to the production of amorphous powder, amorphous ribbons were produced through melt-spinning technique. Later on these melt-spun ribbons were converted into the Fe- amorphous powder with the help of high-energy ball milling. Details of the above mentioned synthesis processes are given in the following sections below:

2.2.1 Thermal evaporation of Au/Cu multilayers

Thermal evaporation is a technique in which a source material is evaporated in vacuum at high temperature and then condenses directly onto the substrate in the form of thin films [152]. Substrate is placed above at a certain distance from the source material. Source materials with low melting points are generally preferred in this technique. The materials to be evaporated are kept in a boat or resistive coil connected to the heating source. Boat or resistive coil is made up of refractory materials such as W, Nb, Mo, and Ta, so as to sustain high heating temperature. In order to evaporate a desired material, a boat or resistive coil is heated to a very high temperature with the help of direct current source. The entire process is done in a vacuum chamber evacuated at pressure ~10^{-4} to 10^{-6} Pa. The vacuum in the chamber facilitates the evaporated material to reach upto the substrate. A schematic of the entire thermal evaporation process is represented in figure 2.1.

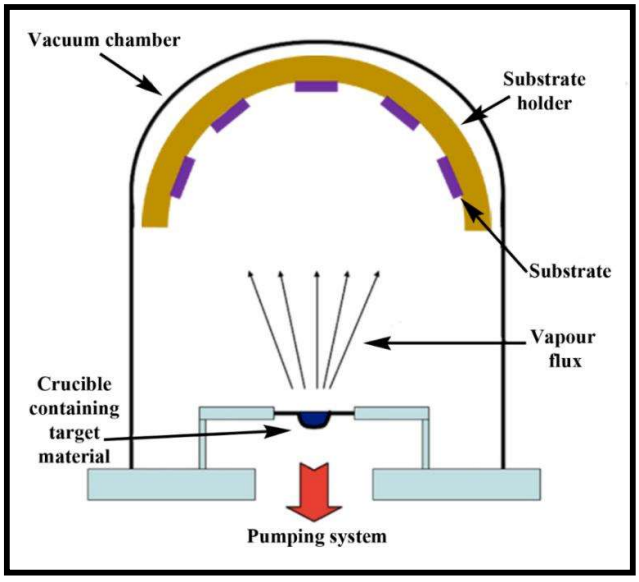

Figure 2.1: *Schematic of a thermal evaporation chamber.*

In this thesis work, thermal evaporation was carried out for two samples, whose details are provided in the table 2.1. The sequence of layer deposition in sample 1 was exactly reversed in sample 2 as is given in table 2.1, and the substrate (polycrystalline Si) was same for both

the depositions. Cleaning of substrate is done by the standard process (level-I). In this process the polycrystalline Si substrate is dipped into the beaker containing warm acetone (kept at 55 °C on a hot plate) and it is left for 10 min. Afterwards, substrate is removed and it is placed in a beaker containing methanol for 2-5 min. Subsequent to this the substrate is rinsed well in DI (De-ionised) water and it is dried in blowing nitrogen. 325 mL DI water in a Pyrex beaker is added with 65 mL NH_4OH (27%) and then it is heated to 70 °C on a hot plate. The hot mixture is removed from hot plate and 65 mL H_2O_2 (30%) is added to the solution. Solution starts bubbling vigorously after 1-2 min, indicating that it is ready for use. The substrate is soaked in the solution for 15 min followed by washing it in running DI water. In order to strip off the native SiO_2 layer present on the substrate, the substrate is soaked for 2 min in a polypropelene beaker containing 480 mL of DI water with 20 mL HF. The substrate is removed and rinsed again in running DI water followed by drying in blowing nitrogen. Now, the cleaned substrate pieces are transferred to the deposition unit from the cleaning room and it is ready for thin film deposition. Rest of the details are given in chapter 3 and chapter 4 of this thesis.

Table 2.1: *Details of the Au/Cu multilayer samples.*

Sample designation	**Substrate Material**	**Thin Film Material**	**Multilayer Sequence**	**Each layer Thickness (nm)**
Sample 1 (40TAu)	Polycrystalline Si	Au and Cu	Poly-Si/Cu/Au/Cu/Au	~ 40
Sample 2 (40TCu)	Polycrystalline Si	Au and Cu	Poly-Si/Au/Cu/Au/Cu	~ 40

2.2.2 Pulsed laser deposition of $Li(Ni,Mn)_xO_y$/Nb-$SrTiO_3$ thin films

Pulsed laser deposition (PLD) is a technique commonly used for thin films deposition of various materials at high temperature [220]. This technique is so versatile that there is almost no restriction onto the target material used for the growth of the thin films. In this technique a high-power pulsed laser is directed towards a target material. The high impact of the pulsed laser decomposes the target material.

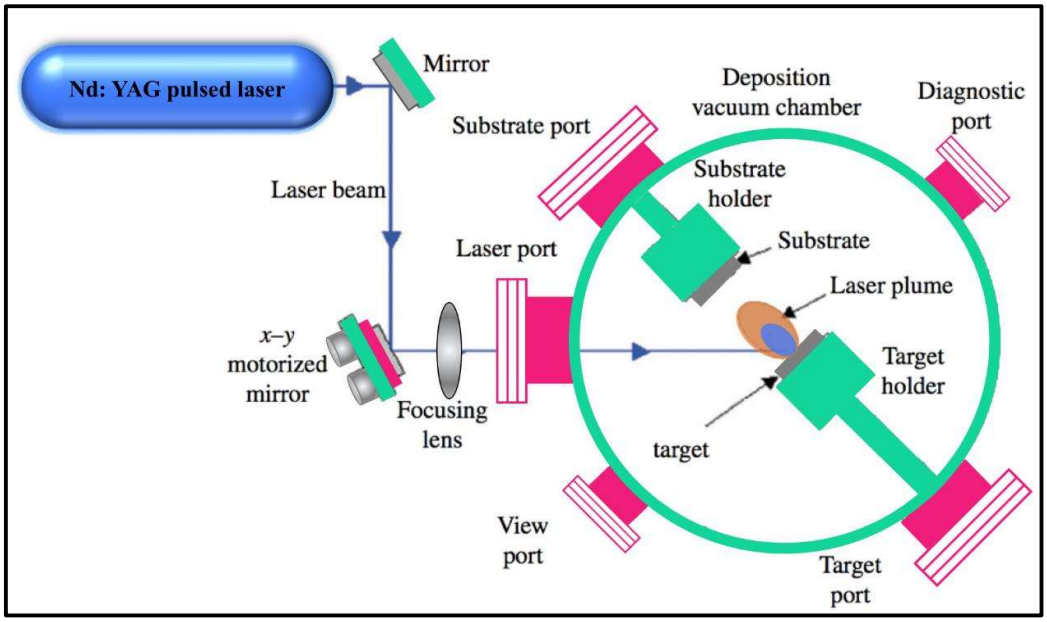

Figure 2.2: *Schematic of a pulsed laser deposition unit.*

This decomposition process raises the temperature of the target material, which then transforms it into the vaporized plasma plume. The generated plasma plume interacts with the nearby substrate and the target material gets deposited onto the substrate. The chamber of the PLD unit is evacuated at an ultra-high vacuum (UHV). Additionally, a controlled atmosphere can also be created inside the chamber with the help of some backfilled gas(s). PLD technique can be frequently utilized for the deposition of various oxides. In this case, generally oxygen is used as a background gas because it helps in the complete oxidation of the material, the oxide form of which is being deposited. A schematic describing the

working principle of PLD process is shown in figure 2.2. In this thesis work, deposition of Li(Ni, Mn)$_x$O$_y$ (LNMO) thin film on (111)-cut single crystal Nb-doped $SrTiO_3$ (Nb:STO) was carried out using PLD technique. The detailed information regarding synthesis process is specified in chapter 5 of this thesis.

2.2.3 Alloy preparation

In order to prepare $Fe_{58.82}Cr_{11.12}Mo_{1.52}Si_{4.16}B_{15.12}P_{8.88}C_{0.39}$ (at.%) alloy, required stoichiometric quantities of raw materials were melted in a 4 kg air induction melting furnace. Once the complete charge was melted, the liquid melt was poured into pre-heated moulds. The cast alloys produced after each heat were chemically analyzed by wet chemical analysis. After confirming the chemical composition, these alloys were further processed.

2.2.4 Melt spinning

Cast alloys were melt spun to produce ribbons in a melt spinner (M/s Vacuum Technologies, Bangalore). Required quantity of the cast ingot was sliced and placed in a quartz crucible, which was fixed properly within the induction coil. The nozzle of the quartz tube was aligned such that the melt flowed on to rotating Cu wheel when ejected. The quenching wheel was water-cooled and was finely polished prior to melt spinning. Chamber was evacuated to 10^{-1} bar and was flushed with high purity Ar-gas prior melting. Wheel speed was maintained at 2500 rpm during the experiment and an ejection pressure of 15 psi was used to eject the melt. Melt spinning produced ribbons of 20 mm width and 40 μm thick.

2.2.5 Ball milling

Vibratory cup mill (Pulverisette 9, M/s Fritsch) was used to grind the ribbons to produce powder. Milling was done at a stretch of 2 min and was given a break for two min before next milling to avoid any heating of the ribbons. The cycle is repeated for 15 times. Powder

thus produced is sieved and the 38 -65 μm size fraction is separated. The flow ability of the powders is measured in Hall flow meter (Make: Alcan metal powder). These powders exhibited flow ability of 50g/s. Subsequently the powder is used as feed stock for thermal spraying.

2.2.6 Thermal spraying (HVOF)

Coatings of the amorphous powder with nominal composition $Fe_{58.82}Cr_{11.12}Mo_{1.52}Si_{4.16}B_{15.12}P_{8.88}C_{0.39}$ (at.%) was deposited via High Velocity Oxy-Fuel (HVOF) spraying (model-HIPOJET-2700, MEC, India) onto cold rolled close annealed (CRCA) mild steel substrate. The coatings produced by HVOF method possess low porosity and high adhesive strength owing to the extremely high velocity encountered by in-flight powder particles. In addition, a fairly high cooling rate in the range of 10^4 -10^5 K/s, associated with this process, promotes formation of amorphous structure.

Before depositing the coating onto the substrate, the mild steel substrate surfaces were polished with 120 grit SiC abrasive paper, it was grit blasted using 24 grit silica beads and then it was subjected to ultrasonication in ethyl alcohol to clean the surface and avoid any contamination. HVOF process parameters for deposition of coating of the ball-milled powder are given in table 6.2 (Chapter 6).

2.3 Cross-section specimen preparation for TEM

The preparation of cross-section specimen is essential for investigating the interfaces in TEM. Cross-section specimen is itself a special kind of self-supporting disk. Mastering of this preparation technique is very important in order to study interfaces in materials. Sample preparation is considered to be the most complicated and limiting component in TEM investigation. Another limitation is its insensitivity towards the structural and chemical variations of the specimen in a direction parallel to the electron beam. Therefore, it is very important to prepare a cross-section specimen in such a way that the interface is parallel to

the electron beam direction in order to look at the variations in the structure and chemistry in a transverse direction to the interface.

Steps for preparation of cross-section specimen begin with the cutting of the layered sample into many pieces of appropriate dimensions. Then the two pieces are glued together like a club sandwich. This is done in order to create multiple interfaces of the same type. This sandwiched piece is then sectioned into the thin slice. The most critical step in this process is to apply the glue before sandwiching the two sections. The glue is the combination of epoxy and resin in the ratio 5:1. Curing of glue requires heat treatment (temperature ~ 110 ^{o}C) for 30 min approximately. There are several epoxies available, which can be cured at low temperatures. While applying the epoxy, its layer thickness should be thin enough for providing the good adhesion. At the same time, it should not be so thin that it is completely eroded away during ion milling. Afterwards the glued sections can be cut down in the form of 3 mm rods with the help of an ultrasonic drill. Alternatively, the samples are cut into such a dimension that it can be encased into the 3 mm thin walled tube. This filled tube is then sectioned into the 3 mm disks. In this method, the periphery of the 3 mm disk is a metal support to the specimen, which provides the mechanical stability. The advantage of multiple interfaces is that it almost guarantees an electron transparent region at an area of interest after ion beam thinning.

2.3.1 Au/Cu multilayer thin films specimen preparation

All the multilayered Au/Cu thin film samples have been converted into the cross–section TEM specimens by following a conventional technique as shown in figure 2.3. The conventional method includes sandwiching the top-sides of the films together with glue (gatan glue), the sandwiched piece is inserted into the brass tube of 3 mm external diameter. This sandwiched piece inside the brass tube is again stuck with the inner wall of the brass tube by application of gatan glue. The 3 mm brass tube with sandwiched piece is then cut

into thin slices of 250 µm thickness. Subsequently, the 250 µm slice is ground to 80 µm thickness with the help of polishing paper. This 80 µm thin specimen is then loaded in the dimpler/grinder in order to dimple it upto a thickness of 20 µm. Furthermore, this 20 µm thin specimen is loaded inside the ion miller so as to mill it until the perforation appears in the glued region. Utmost care is taken while ion milling the specimen in terms of keeping the gun angle and gun current.

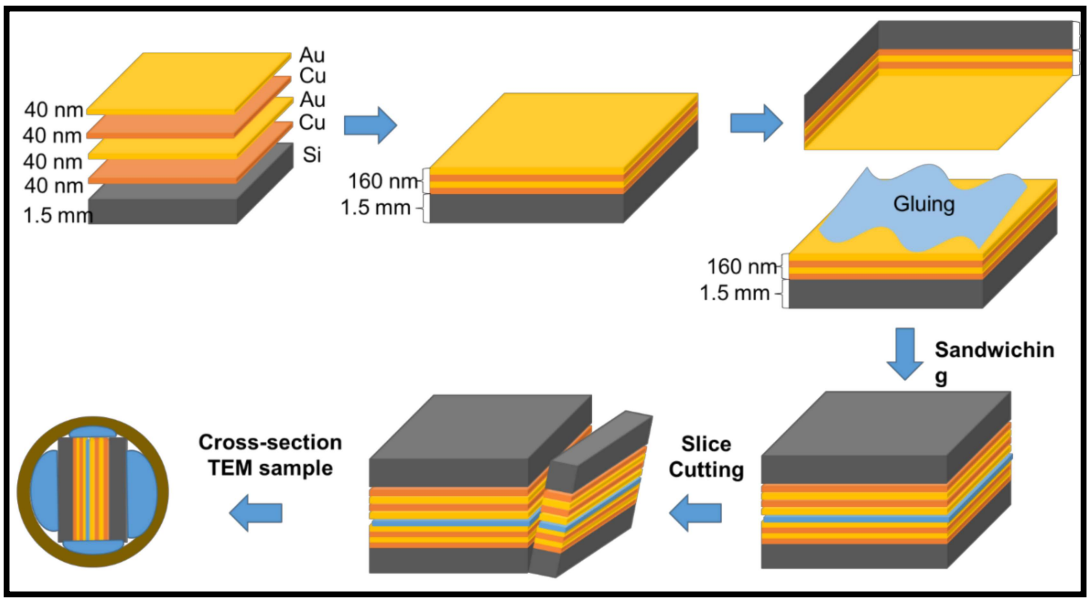

Figure 2.3: *Schematic sequence for the Au/Cu multilayer (40TAu) cross-section specimen preparation. The same method is applied for the 40TCu specimen preparation, only the deposition sequence is reversed.*

In the present case, gun angle is kept at 5º for 30 min, 4º for 1h and 3º for rest of the time till perforation. Ion beam polishing was carried out with Gatan PIPS with Ar-ions operated under 5keV.

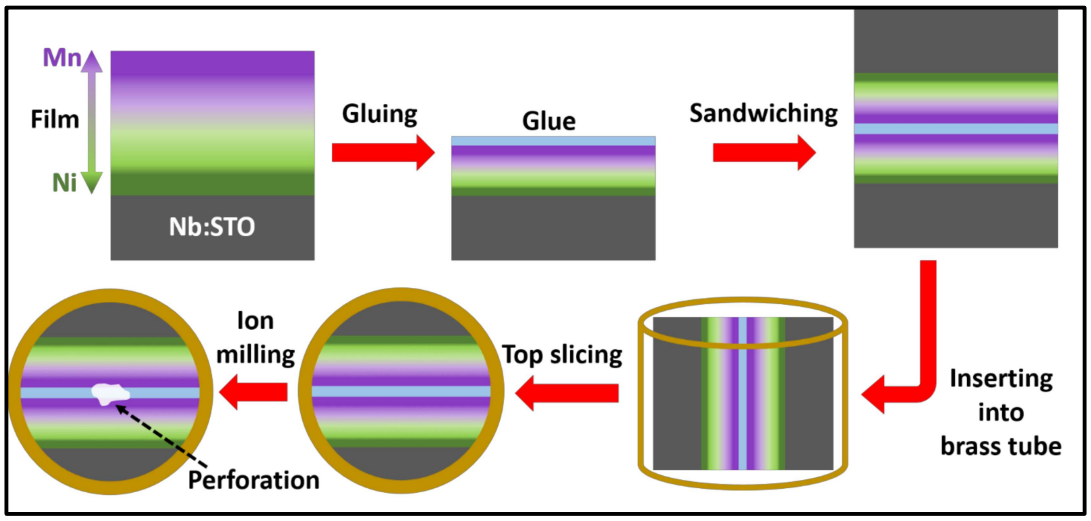

Figure 2.4: *Schematic sequence for the LNMO/ Nb:STO cross-section specimen preparation.*

2.3.2 LNMO/ Nb:STO core-shell thin films specimen preparation

Steps for the preparation of cross-section TEM specimen of compositionally graded LNMO/ Nb:STO core-shell thin films is shown in figure 2.4. This is also performed in a similar way following a conventional technique as discussed in the section 2.3.1.

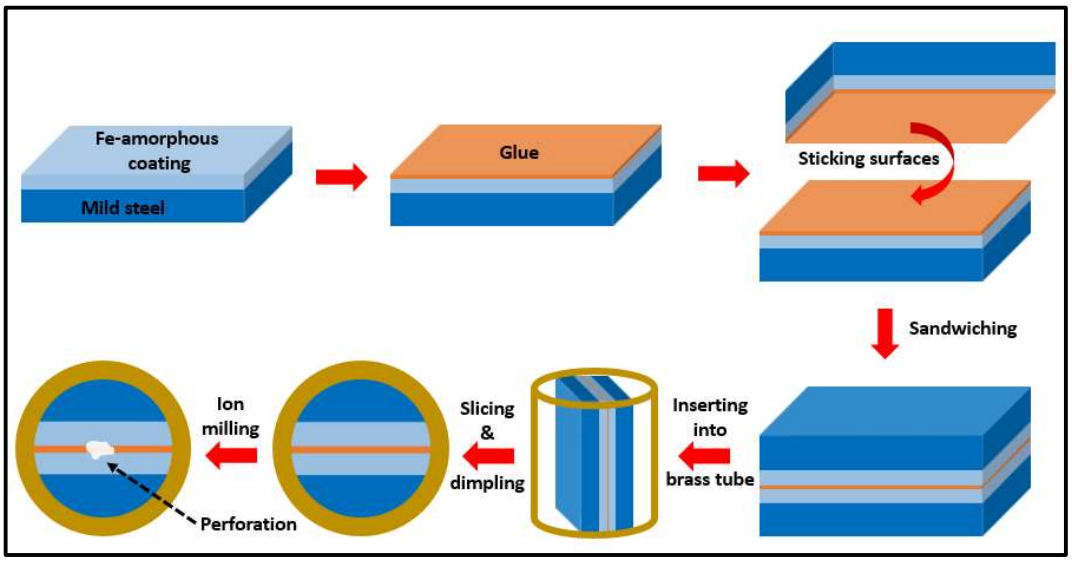

Figure 2.5: *Schematic sequence for the cross-section specimen preparation of Fe-based amorphous/mild steel coatings.*

2.3.3 Amorphous-steel nanocomposite/ mild steel coatings specimen preparation

The cross-section specimen preparation of amorphous nanocomposite steel coated on mild steel was also done through a conventional method in a similar manner as specified in section 2.3.1 and 2.3.2 of this chapter. Key steps for cross-section TEM specimen preparation are demonstrated in figure 2.5.

2.4 Structural characterization

Once the sample preparation is over then the important task is to characterize the samples. Selection of characterization technique depends on the type of information desired from the specimens. In this study, conventional x-ray diffraction (XRD) technique is applied to identify the crystal structure, crystallite size and phase evolution in the amorphous-steel nanocomposite materials. Grazing incidence x-ray diffraction (GIXRD) technique is used for the characterization of Au/Cu multilayer thin films samples. Scanning electron microscope (SEM) is used to extract the information related to shape, size, microstructural features, and phase distribution in the amorphous-steel hard coatings. However, the information, which could not be extracted from the SEM owing to its limited resolution was dealt with TEM. TEM is a very powerful instrument for resolving the materials information up-to a level of atomic dimensions. Diffraction contrast imaging (DCI) was performed on the Au/Cu multilayers, LNMO thin films, and amorphous-steel nanocomposite materials so as to distinguish the dissimilar phases present in them based on their individual diffraction conditions. HRTEM studies revealed the distribution of defects, order-disorder transformations, and structural dynamics at surfaces/interfaces in all the three material systems. On the basis of the atomic number, HAADF-STEM imaging aided the recognition of the chemical species present in the Au/Cu multilayers and LNMO/Nb:STO thin films. Distribution of chemistry in the Au/Cu multilayers and LNMO/Nb:STO thin films was investigated through XEDS line and area mapping.

However, in order to identify the low atomic number element such as lithium (Li) in the LNMO/Nb:STO thin film, electron energy loss (EELs) spectroscopy was done. Characterization techniques described above are discussed in detail below:

2.4.1 Grazing incidence X-ray diffraction

As described in the section 2.2.1, the two samples with designation 40TAu and 40TCu were synthesized through thermal evaporation technique. In order to investigate the phase evolution, crystallite size, strain and microstructure in both of the Au/Cu multilayer samples, GIXRD was performed. The geometry of the GIXRD follows the in-plane diffraction condition. This was performed in a high resolution XRD (Rigaku Smart Lab operating at 45kV and 200mA) with a Cu $K_{@}$ X-rays with a wavelength = 1.54 Å. Both the samples were scanned from 10° to 90° degrees with a step size of 0.02^0. However, while deciding the angle of incidence, several incidence angles ranging from 0.1 to 3° were tried. Maximum intensity of peaks was found at 0.45^0 incidence angle.

In addition, the coherently scattered domain size has been estimated with the help of Scherrer equation whereas average strains have been computed based on Williamson-Hall equation. A careful observation of the individual peaks given in figure 3.2 (Chapter 3) indicated significant broadening. The broadening of peaks after taking care of instrumental broadening has been utilized for estimating crystallite size and presence of non-uniform strain in the film. The size of the crystallites present in the multilayered 40TAu thin films was calculated from diffraction peak broadening utilizing the Scherrer equation.

$$d = \frac{\mathrm{k} * \lambda}{\beta * cos\theta}$$

where, k is a constant (k=0.91), λ is Cu-Kα (λ = 0.154 nm) wavelength, β is the broadening of the full width at the half maximum (FWHM) and θ is the Bragg's angle. The average strain present in the multilayer thin film is measured from a plot of Williamson-Hall

equation as mentioned below:

$$\beta * cos\theta = \frac{k * \lambda}{d * cos\theta} + 4 \in * sin\theta$$

where $\in$ is strain and d is the crystallite size.

2.4.2 X-ray diffraction

Structural investigation of the amorphous phase and the nano- crystallites embedded in the amorphous matrix in the melt-spun ribbon, melt-spinning followed by ball milled powder and in thermal spray (HVOF) coating samples were carried out by X-ray diffraction (MiniFlex600, RIGAKU) using Cu-K_α radiation. The operating conditions were kept at 40 kV of accelerating voltage and 15mA of current. All the samples were scanned from 2θ to 100^0 angle with a step size of 0.02^0. The melt-spun ribbon pieces were wrapped inside a cello-tape and were held inside an annular aluminum holder in such a manner that both sides of the ribbon pieces could be exposed to the x-ray source. Utmost care was taken in case of powder sample in order to smoothen its surface in an aluminum holder with 200 μm depression. Coating sample was directly mounted from the substrate side in an aluminum holder having 500 μm depression. Coating surface was kept upside so that x-rays should predominantly interact with coating surface. All the three samples were loaded horizontally and were kept side by side on a specimen stage equipped with six slots. The interpretation of x-ray diffraction patterns was done with the help of JCPDS/ICDD data cards.

2.4.3 Scanning electron microscopy (SEM)

Scanning electron microcopy is a type of electron microscopy technique, which is widely used to characterize the morphology and microstructure of nanostructured materials and thin films. It is generally used to study the surface texture, topography, particle size distribution and chemical composition.

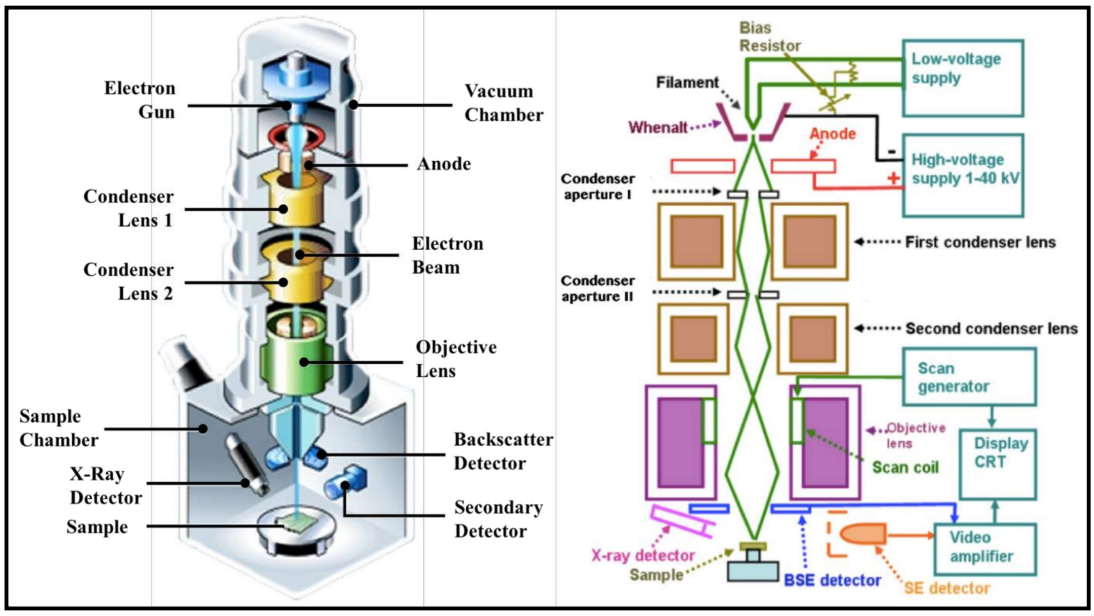

Figure 2.6: *Schematic of SEM* ***a)*** *Front half section,* ***b)*** *Electron beam trajectory* [221].

The information that is revealed through SEM is basically related to the surface and subsurface regions of the specimen. The basic components of the SEM architecture consist of vacuum chamber, electron gun, condenser lenses, objective lens, sample chamber, detectors and sample stage as shown in figure 2.6a. The electron gun is a source for electron beam with an energy ranging from few hundred eV to few keV. Electromagnetic condenser lenses are used to converge the electron beam (<5 nm diameter). The high-energy electron beam raster on the surface of the sample with the help of scan coils in order to scan the sample. Additionally, the high-energy electron beam also penetrates inside the sample surface up-to few micrometers and undergoes electron-matter interactions. These electron-matter interactions can be elastic and inelastic in nature. Depending on the elastic and inelastic electron-matter interactions, many useful signals such as secondary electrons (SEs), X-rays, backscattered electrons (BSEs), and cathodoluminescence are generated.

A schematic representing the SEM along with the detectors for various signals are given in figure 2.6b. Backscattered electrons are the result of elastic interactions and they are

reflected from the materials surface with high energy. Therefore, the contrast in the BSE image can easily be distinguished on the basis of atomic numbers of the elements. Secondary electrons are ejected from few nm depth of the specimen surface due to the inelastic interaction of the beam electron with the specimen. The energy of SEs is comparatively lower than the BSEs. So, BSEs are used to study the surface topography of nanomaterials and thin films. Each of these signals are collected by their specific detectors so as to form images on the display monitor. In the present work, microstructure and composition of the ball milled powder and the hard coating were studied. Sample of ball-milled powder was prepared by dispersing a few mg of powder in a solution of ethanol and hexane. Subsequently, it was drop-cast onto a pre-cleaned Si wafer. Similarly, the surface of the hard coating was cleaned by acetone solution. The images from both the samples were obtained using Ultra 55 FE-SEM Karl Ziess equipped with EDS.

2.4.4 Transmission electron microscopy (TEM)

Transmission electron microscopy is another advanced characterization technique through which a highly magnified image of nanostructured materials and thin films can be obtained using parallel electron beam. The high-energy electron beam is accelerated at a voltage of ~ 200 kV. However, energy of the electrons can be controlled by calibrating the TEM to other voltages in the range of 80-300 kV. The operating principles of TEM are same as visible light microscopy, only the electrons are utilized in TEM instead of light. Light microscopy involves the wavelength of visible light; therefore, it is limited in terms of image resolution. The resolution of the visible light microscope is ~ 200 nm. In this context, TEM is far superior to light microscope as electrons can be tuned into much shorter wavelength in order to give high resolution. The resolution in optical microscope is governed by Rayleigh criteria:

$$\theta = sin^{-1}\left(\frac{1.66 * \lambda}{d}\right)$$

where *'λ'* is the wavelength of the radiation and *'d'* is aperture diameter.

The resolution of TEM is dependent on the wavelength of the electron beam under consideration. The non-relativistic wavelength of electron is calculated with the help of de-Broglie relationship:

$$\lambda = \left(\frac{h}{m*v}\right)$$

where *'h'* is the Plank's constant , *'v'* is the velocity of the electron and *'m'* is the mass of the electron.

The wavelength of electron beam accelerated at 200 kV is ~ 0.0025 nm as per de-Broglie relationship. With this small value of wavelength, the spatial resolution of the TEM becomes pretty high. Fundamentals of TEM imaging involve the quantum mechanical treatment of the interaction of the beam (electrons) with the atomic potentials of the materials. The electron beam while getting transmitted through the specimen gets diffracted or scattered with change in phase. The transmitted or exit wave becomes an object for the underlying projector lens. Projector lens amplify the exit wave signal and project it on to the fluorescent screen as an image. Figure 2.7 depicts the overall assembly of a TEM and its inside view as a schematic representation. Figure 2.8 shows the path of an electron beam.

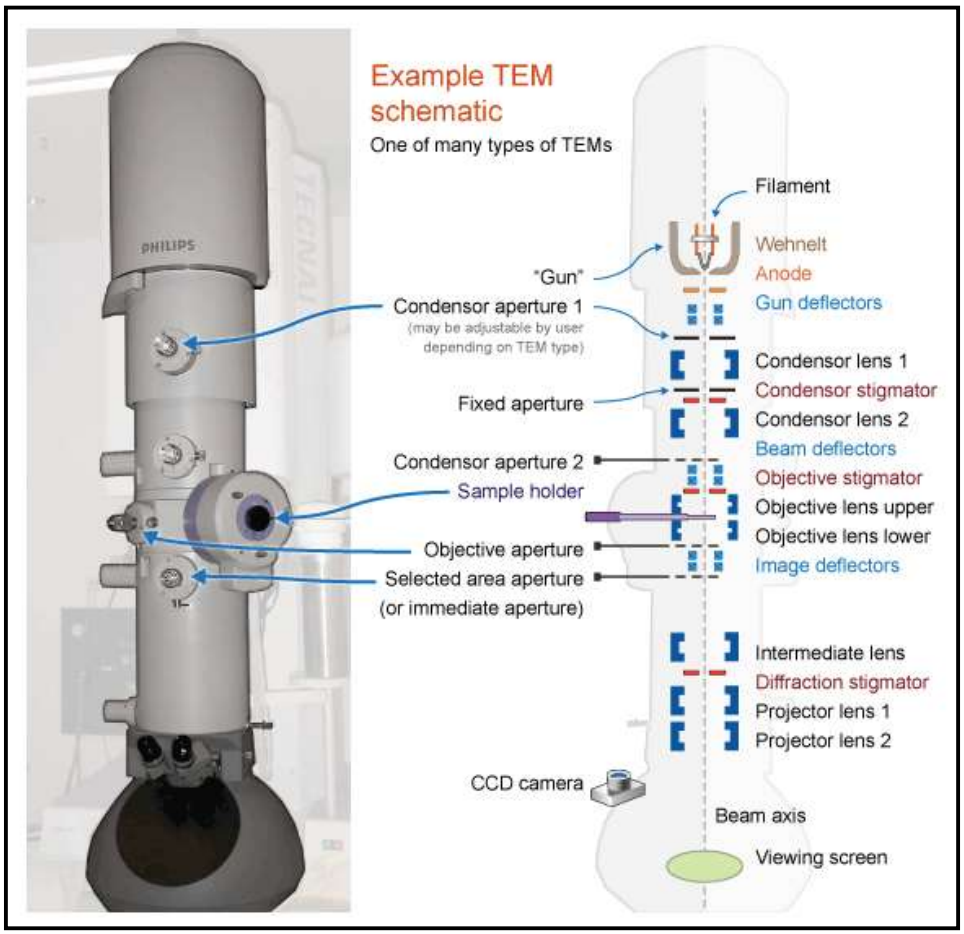

Figure 2.7: *Schematic of a TEM* ***a)*** *overall cabinet assembly and,* ***b)*** *inside view.*

Thesis work involves the investigation of Au/Cu multilayer thin films, Fe-based amorphous ribbon, powder and coating using Tecnai G^2 T20 (C_s = 1.2 mm) TEM operated at 200 kV equipped with HAADF and STEM-EDS detectors. Moreover, the diffraction contrast imaging and diffraction experiments of LNMO/Nb:STO thin films were investigated through JEOL 3010 TEM operated at 300 keV. Additionally, negative aberration corrected phase contrast imaging, electron energy loss spectroscopy, STEM-EDS mapping and line scan of the LNMO/Nb:STO thin film cross section was carried out in a FEI Titan with super twin lens (C_s=1.2 mm) operated at 300 kV. Specific details of the TEM techniques used for each of these samples are stated in the experimental section of the chapters 3, 4, 5, and 6 subsequently.

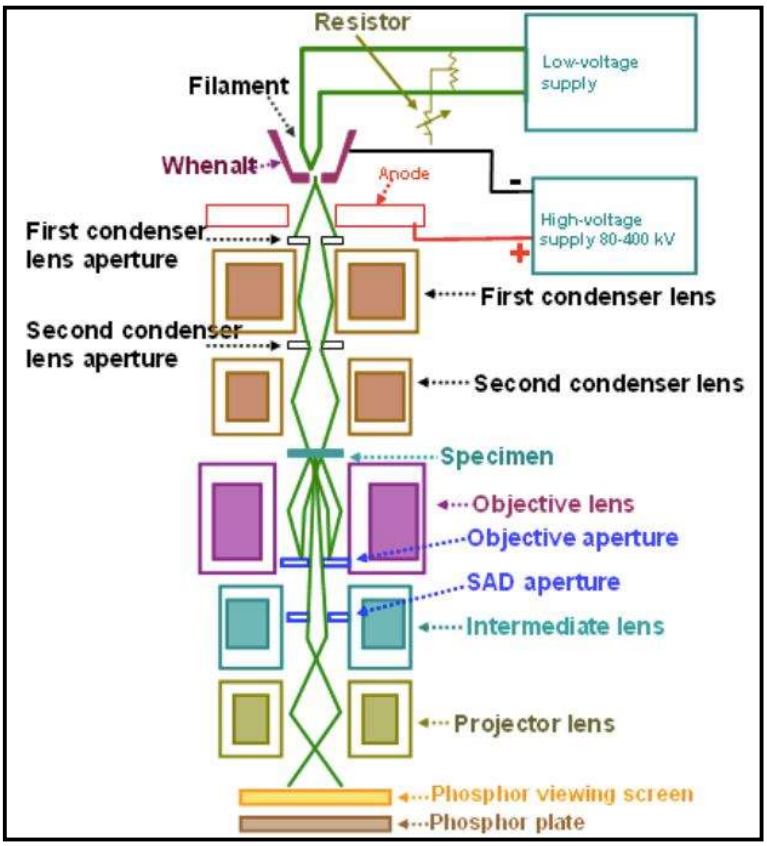

Figure 2.8: *Schematic representing path of an electron beam in TEM* [221].

2.5 Computational techniques

It is not always straight forward to analyze the experimental results manually. Major part of the results in the present work involves numerous calculations and complex structural geometries of the crystals, hence, it is essential to the take the help of computational techniques. A brief discussion related to the computational techniques utilized in this work is mentioned in the subsections below:

2.5.1 XRD pattern simulation

From the phase diagram of Au and Cu, it is quite clear that the structural parameters of tP4, oP8, oI40 and cP4 structures are very close. Therefore, it is quite difficult to ascertain their presence in the nanostructured Au/Cu multilayers thin films. Since the deposition of Au/Cu multilayers was done in non-equilibrium conditions, it is even more difficult to confirm

their presence through experimental GIXRD pattern. In order to resolve this issue, XRD patterns of tP4, oP8, oI40 and cP4 structures are generated through data simulations. Structure factor, multiplicity factor and Lorenz-polarization factor were calculated for each of these equilibrium and non-equilibrium structures. Such heavy calculations involved computational help. The relative intensities were determined with respect to the diffracting planes for each structure. Later, these relative intensities were plotted against twice the Bragg angles in order to generate the simulated XRD pattern. Each of these simulated XRD patterns were then compared with the experimental GIXRD pattern so as to conform the evolution of tP4, oP8, oI40 and cP4 phases in the Au/Cu multilayer thin films. Such descriptions are made in chapters 3 and 4 of this thesis.

2.5.2 MATLAB

In the section 6.5 (chapter 6) of this thesis, thermodynamic phase stability studies of Fe-Cr-Mo alloys have been carried out by computational techniques. Formation enthalpies for the binary Fe-B and Fe-C, and ternary Fe-Cr-Mo system have been calculated using Miedema's model. MATLAB software is used to perform such complex calculations and their execution.